THE SENSITIVITY OF THE NUMERICAL SIMULATION TO OROGRAPHY SPECIFICATION IN THE LOWRESOLUTION SPECTRAL MODEL—PART II: IMPACT OF THE SMOOTHED OROGRAPHY AND RIPPLES ON SIMULATIONS

Ni Yunqi (倪允琪)

Department of Atmospheric Sciences, Nanjing University, Nanjing

Bette L. Otto-Bliesner and *David D. Houghton*

Department of Meteorology, University of Wisconsin, Madison, WI 53706, U.S.A.

Received November 10, 1985

ABSTRACT

In order to investigate the impact of the smoothed orography and the spurious orographic ripples on simulations in the low-resolution spectral model, three different numerical tests, that is, the unsmoothed orography scheme, the smoothed orography scheme and non-ripples scheme are performed. In this paper, the model used by us is the same as Part I except for orographic specification.

The results from simulations indicate that, as far as the climatic simulation is concerned, some aspects of the simulated stationary disturbances, zonal and meridional wind, temperature and precipitation in the low-resolution spectral model with properly smoothed mountains are significantly improved, especially in winter hemisphere.

The deep ripples in the model with the unsmoothed orography produce spurious high pressure regions at the surface with subsidence, and suppress rainfall, causing an unrealistic splitting of the precipitation area in northern winter and summer. Removal of the deep ripples by using the special procedure for smoothing topography allows a strong upward motion in the ripple area with heavy rainfall, eliminating the unrelistic split in the precipitation area.

I. INTRODUCTION

The representation of orography in a numerical model is a very complex problem, about which there has not been a certain conclusion (Gates, 1984). In numerical models, there are two different orography specifications in whatever vertical coordinates: one is the smoothed orography incorporated gridly or spectrally into a model as a lower boundary condition for the geopotential (for example, McAvaney et al., 1978); the other is the full mountains directly incorporated into a model in the grid space or the wave space as a low boundary condition of the model (for example, Otto-Bliesner et al., 1982). In general, the response of the atmosphere to a mountain barrier depends upon the mountain's height and width, the speed, width, orientation and latitude of the incident flow. Obviously, the full mountains basically remain the actual mountain's height, width, slopes and so on. Therefore, the simulation of atmosphere response to orography should be reasonable by using the model with the full mountains. But conservation principles are not enforced over steep mountain slopes since the original slopes of mountains are remained (Arakawa and Lamb, 1981). However, this conservation principle profoundly affects the behavior of both transient and stationary flow patterns,

What is more important is that the computational instability is easily generated since the σ coordinate levels are very steep over the steep slope side of a mountain in the unsmoothed orography model with the σ vertical coordinate (Ni, 1986). And this may lead to considerable error of the pressure gradient force terms. The deficiency of the smoothed orography in the model apparently is to distort an actual mountain's height, extent and slopes. It is difficult to accurately simulate the atmosphere response to real topography, especially the effect of the mountain with steep slopes on the vertical motion although the smoothed orography eliminates the effect of steep-slope mountains on the computation of model. Apparently, there are both advantages and disadvantages in each scheme. But it remains uncertain which one is better and that is one of the questions the present study intends to deal with.

There is a special problem about orographic treatment in the spectral model, that is, the spectral transform of orography produces orography with negative heights (called "ripples"). Obviously, the ripples in the spectral model also distort actual orography. Note that steep slopes of orography are associated with strong ripples. Otherwise, ripples are weak. Therefore, Bourke et al. (1977) emphasized that in their spectral model, orography was so smooth that spurious oceanic "ripples" should not exceed 60 meters. However, the strongest ripple exceeds 600 meter in our low-resolution spectral model with full mountains. But so far, the effect of ripples on simulation is not clear (Bourke et al., 1977). In this paper, we attempt to study this problem.

In order to study problems described above, unsmoothed orography, smoothed orography and non-ripples schemes are considered in Section II, Section III compares the results with full orography and smoothed orography in the model. We attempt to isolate the effects of ripples on simulated results in Section IV. A summary and conclusions follow in Section V.

II. SPECIFICATION OF OROGRAPHY IN THE MODEL

In this study, we use the model and the parameterizations of all the physical processes in the model as same as the model used in Part I (Ni et al., 1987) except for orographic specifications.

Orography is incorporated spectrally into the model with triangular truncation at wavenumber 10 (Ni et al., 1987). Due to truncation, the height of mountains in the spectral model is generally lower than actual height and, in addition, there are negative heights of orography, called "ripples", due to the nature of truncation in the spectral formulation.

In order to investigate impact of the smoothed orography and the spurious orographic ripples on simulations, three different specifications of orography are considered. The detailed description is as the following:

Case 1, "full" ("unsmoothed") mountain case (control case, Fig. 1a): One degree latitude-longitude orography (Jenne, 1975), modified over the Antarctic and Greenland ice caps, is spectrally truncated at wavenumber 10 and incorporated directly into the model. The heights of full mountains are close to those of actual mountains and there are many negative-height areas in the model, especially in the oceans. The maximum absoluted value of negative height is 663 m. This specification incorporates the basic low-resolution effects of the model without other considerations.

Case 3, smoothed mountain case (Fig. 1b): A two-dimensional nine-point filter is applied to the height field of orography used in the full mountain case. The heights of smoothed mountains are lower than those in the full mountain case, and the absolute

value of negative heights are smaller than those in the latter as well . The specification helps to identify the effects of a general smoothing in the orography forcing.

Case 4, no-ripple case (smoothed mountains): An alternate formulation is used for smoothed mountains. The negative heights in the "full" mountain case are set to zero, and then the entire field is smoothed by using a two-dimensional nine-point filter. Then the field is transformed from grid space to wave space and back. The procedure as described above is repeated five times. The final results is a "no-ripple" height field for orography on the transform grid meaning that there are essentially no points left with negative heights. The heights of orography in this case are similar to those in the smoothed mountain case, and there is only one grid to be -2 meter. This specification makes it possible to isolate the special effects of the "ripples" (see Fig. 1c).

The topography characteristics of these schemes are compared in Table 1. The heights of mountains in the "full" mountain case are closest to the actual heights of mountains. The gradients $|\nabla_X Z|$ (land or ocean) and $|\nabla_Y Z|$ (land or ocean), the number of ripple grids and the mean values of negative heights in the full mountain case are the largest of the three cases. Conversely, $|\nabla Z|$, the number of ripple grids and mean absolute values of negative heights in the no-ripple case are smallest. Even though the heights of mountains in no-ripple case are close to those in the smoothed mountain case, $|\nabla Z|$, the number of ripple grids and mean values of negative heights in the no-ripple case are much smaller than those in the smoothed mountain case.

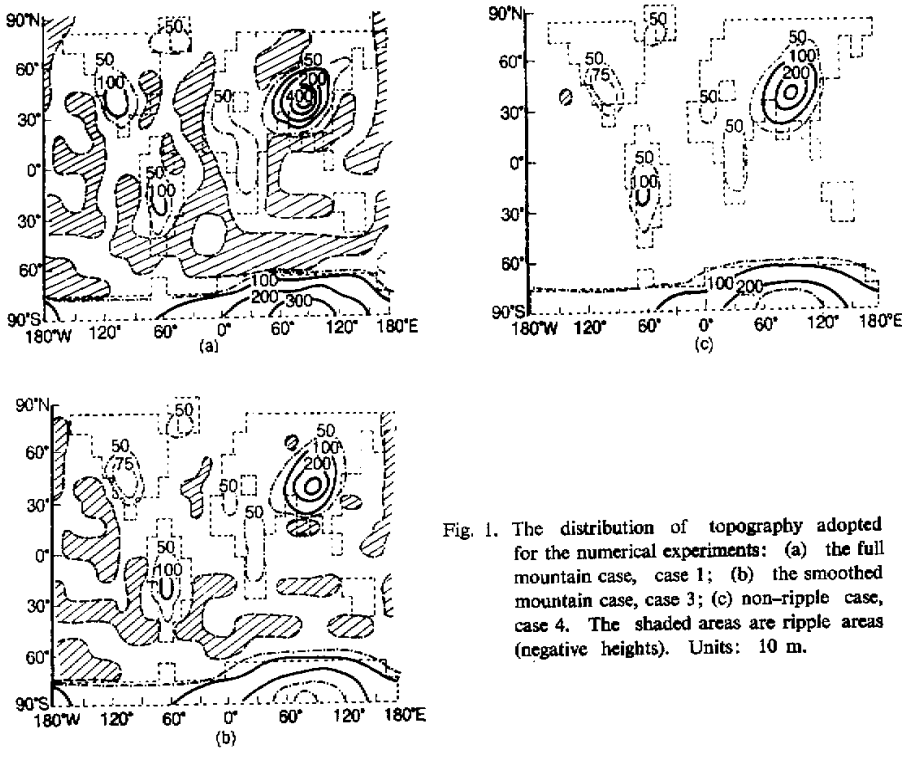

Fig. 1. The distribution of topography adopted for the numerical experiments: (a) the full mountain case, case 1; (b) the smoothed mountain case, case 3; (c) non-ripple case, case 4. The shaded areas are ripple areas (negative heights). Units: 10 m.

Table 1. Basic Characteristics of Different Orography Specifications (∇_x and ∇_y Refer to Gradients in the x and y Directions, Respectively)

Scheme	Mean Height Gradients (m/km)				Maximum Height (m)	Negative Height Area Characteristics (total grid points 480)		
	$\nabla_x Z$		$\nabla_y Z$					
	Ocean area	Land area	Ocean area	Land area	Z_{max}	Number of ripples	Z min (m)	Z mean (m)
Case 1	0.142	0.325	0.245	0.801	4079	145	−663	−129
Case 3	0.070	0.186	0.118	0.451	3044	102	−200	− 5
Case 4	0.052	0.170	0.098	0.425	2939	1	− 2	− 2

All differences between any case and the full mountain case are statistically tested by using t-test (Chervin and Schneider, 1976) whether they are significant. The t-test used in this part is the same as that in Part I (Ni et al., 1986).

III. COMPARISON OF SIMULATION BETWEEN MODELS WITH THE "FULL" MOUNTAINS (CASE 1) AND SMOOTHED MOUNTAINS (CASE 3)

Results are discussed using the control, Case 1, as the reference.

1. *Northern Hemisphere Winter (December–February)*

The geopotential height difference between cases 3 and 1 at 900 hPa and 300 hPa in northern winter are shown in Fig. 2a and b, respectively. The difference at 900 hPa is significant and exceeds 50 m over Tibet, Siberia and north-western Africa. At 300 hPa, the geopotential height difference exceeds 100 m over Siberia, Iceland and 50 m over the Rocky mountains and South America. The smoothing of the mountains has thus weakened the low over Tibet and the Siberian high in the lower troposphere, strengthened the ridge corresponding to the Siberian high at 300 hPa, and deepened the trough over Iceland. The differences in the Aleutian low area are not significant. The simulation of stationary disturbances with the smoothed topography (case 3) is actually in better agreement with observation.

The zonal wind difference exceeds 5 m/s (three standard deviations) at 900 hPa north of 60°N. To the northeast of Tibet, the zonal wind is weaker while it is stronger over the northwest of Tibet with the smoothed mountains (Fig. 3a). In addition, the zonal wind difference exceeds 5 m/s (three standard deviations) at 300 hPa along the zone from 30°N to 60°N and just north of the equator. The smoothing of mountains, in general, weakens the westerly jet over Asia and intensifies it over North America along the zone from 30°N to 50°N in the upper troposphere. Mountains' smoothing also intensifies the zonal wind in the upper troposphere and weakens it in the lower troposphere to the north of 50°N. The simulated zonal wind in the Northern Hemisphere in case 3 is closer to the observed values than in case 1.

At 900 hPa, the meridional wind difference exceeds 5 m/s and is significant only over the south of Iceland, the east of Rocky mountains and Tibet, while at 300 hPa the meridional wind difference along the zone from 30°N to 60°N exceeds 5 m/s is significant

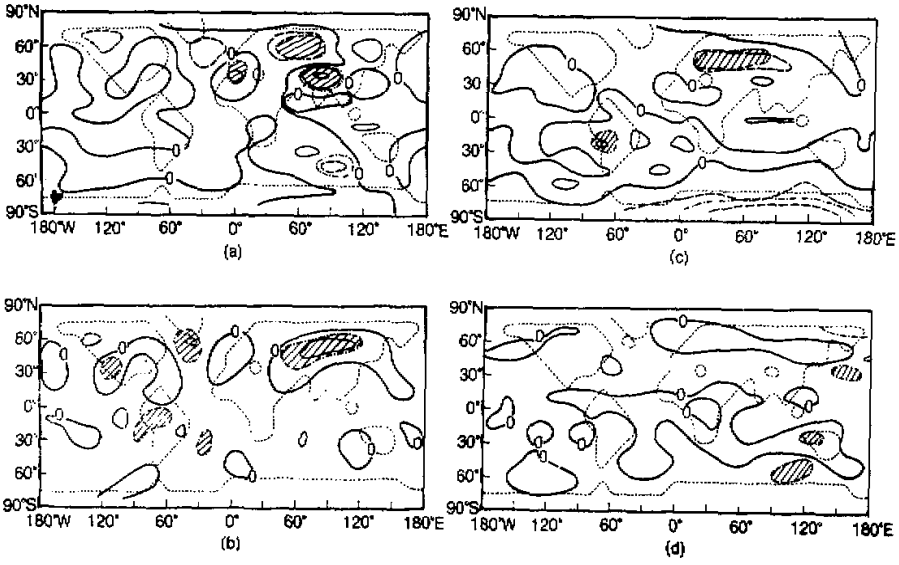

Fig. 2. Simulated geopotential height difference maps (case 3 minus case 1). Contour intervals, 50 m. solid line, positive difference; dashed line, negative difference. Shaded areas are statistically significant at the 5% level. (a) 900 hPa for northern winter; (b) 300 hPa for northern winter; (c) 900 hPa for northern summer; and (d) 300 hPa for northern summer.

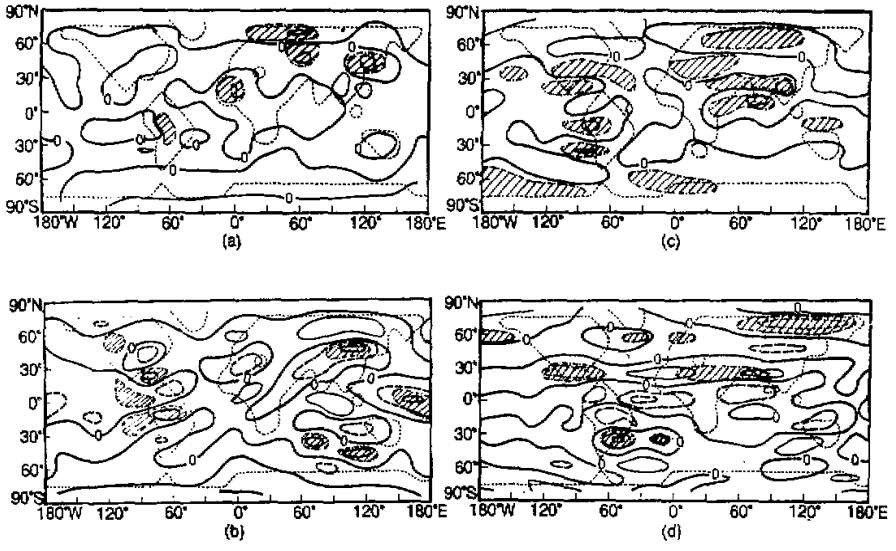

Fig. 3. Simulated zonal wind difference maps (case 3 minus case 1). Contour intervals are 5 m/sec. Solid lines are for positive differences; dashed lines for negative differences. Statistically significant areas at the 5% level are shaded. (a) 900 hPa for northern winter; (b) 300 hPa for northern winter; (c) 900 hPa for northern summer; and (d) 300 hPa for northern summer.

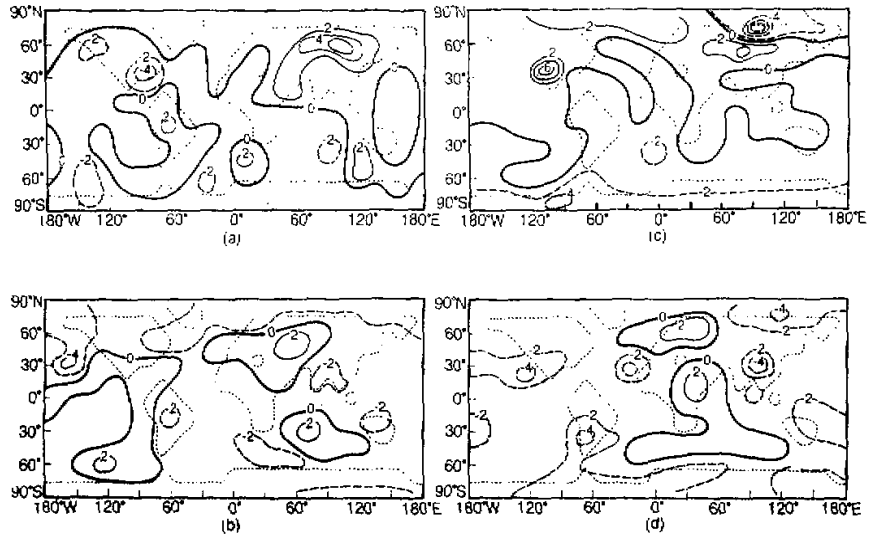

Fig. 4. Simulated temperature difference maps (case 3 minus case 1): (a) 900 hPa for northern winter; (b) 300 hPa for northern winter; (c) 900 hPa for northern summer; and (d) 300 hPa for northern summer.

over South America, North America and the Atlantic Ocean (figure omitted). The magnitudes in the Icelandic low and North America area are increased with the use of smoothed mountains, bringing the simulation into better agreement with observation. The smoothing of the Tibetan Plateau has an influence on the meridional wind mainly in the lower troposphere.

The vertical motion difference at 900 hPa exceeds 0.04×10^{-4} hPa/s over Tibet, India and north Asia which is statistically significant. The influence of smoothed mountains on the vertical motion at 300 hPa is relatively small. The vertical motion field will further be discussed in next section.

The temperature is higher over Siberia, lower over North America and higher over South America at 900 hPa, while at 300 hPa, higher over Europe, lower over North America and South America with the smoothed mountains (see Fig. 4a, b). As with the other variables already discussed, the simulated temperature field is in better agreement with observations with the smoothed mountains (case 3).

Otto-Bliesner et al. (1982) pointed out that the simulated precipitation in the control is heavier than observed but is in the correct areas. We find that the precipitation areas in case 3 are similar to those in case 1, being slightly closer to the observed in case 3; the main precipitation area in Asia is splitted into two parts in both cases: one is in China and the other is in the western Pacific and Indian Ocean, but precipitation in the area between two major precipitation areas is heavier in case 3 than in case 1.

2. *Northern Hemisphere Summer (June—August)*

The geopotential height differences at 900 hPa and at 300 hPa in June—August are shown in Fig. 2c and d. The geopotential height differences at 900 hPa significantly ex-

ceed 50 m only over the zone from 45°N to 60°N and from 0°E to 100°E, Antarctica, and the west coast of South America (the Andes Mountains). However, the difference at 300 hPa exceeds 50 m over Tibet and the east coast of North America but is not significant. The geopotential heights over these areas are reduced in case 3. It is noteworthy that over Antarctica of the Eastern Hemisphere, the smoothed mountains significantly decrease geopotential heights at 900 hPa and a low system is simulated in case 3 instead of the spurious high system in the lower troposphere in case 1 (see Fig. 2c, d). Apparently, smoothing the mountains has more influence on the geopotential heights in winter hemisphere than that in summer hemisphere.

The zonal wind differences exceed 5 m/s only over the southeast of Tibet and the west coast of South America at 900 hPa and over the southern Asia, the northern Asia, the southern North America and the southern South America at 300 hPa and are significant to 5% (Fig. 3c, d). In general, the easterly jet along 20°N from 0° to 100°E, over southern North America at 300 hPa and along 20° N from 30°E to 100°E at 900 hPa are weaker in case 3 than in case 1. The easterly flow over the northern Asia in case 1 is reversed as in case 3. All the simulated zonal wind in northern summer with the smoothed mountains is closer to the observed.

The meridional wind difference is significant, exceeding 5 m/s over the Rocky mountains at 900 hPa and over South America at 300 hPa (Fig. omitted).

The vertical motion difference maps at 900 hPa and at 300 hPa are omitted. The vertical motion differences exceed 0.05×10^{-4} hPa/s only over the Andes Mountains at 300 hPa. However, the difference is significant and less than 0.05×10^{-4} hPa/s over Asia, North and South Americas, and the Atlantic at 900 hPa. This indicates that the smoothed mountain has an obvious influence on the vertical motion only over South America.

Fig. 4c and d shows the temperature differences at 900 hPa and at 300 hPa. The temperature differences exceed 4° over the northern Asia and the Rocky Mountains at 900 hPa, whereas at 300 hPa the differences exceed 4° over the northern Asia, Tibet, the west of the Rocky Mountains, the eastern Atlantic Ocean and the Andes Mountain. In case 3, temperature at 300 hPa reduces over the area described above and over the northern Asia at 900 hPa but increases over the Rocky Mountains at 900 hPa. The temperature field in case 3 is closer to observations, especially for the warm area at 300 hPa.

The difference of precipitation between cases 3 and 1 is similar to that in December—February, and the main precipitation in Asia is split into two parts in case 1: one is in China and the other is in the western Pacific and Indian Ocean, but in case 3, the main precipitation area only appears in Southeast Asia and the western Pacific, and is more realistic.

IV. THE EFFECT OF RIPPLES ON THE SPECTRAL MODEL SIMULATIONS

The ripples influence is studied by comparing the simulation from the full mountain case with both the "smoothed" and no ripple case. Let us look at the area, south of Asia, where the ripple has the largest magnitude and effects are most evident. The deepest ripple point is located at 11.7°N and 90°E in case 1, but this ripple disappears and height of mountains is reduced by smoothing in case 4.

Comparing the vertical motion differences between cases 4 and 1 with ripple areas in case 1, we find that such motion is basically consistent with ripple areas. It clearly shows that the reduced topography heights by smoothing decrease upward motion or

increase downward motion, while the raised topography heights by smoothing increase upward motion or decrease downward motion. According to the results described above, we deduce that the ripples in case 1 have an influence on the simulation of vertical motion, that is, ripples in case 1 decrease upward motion or increase downward motion.

The cross section of the geopotential heights in summer along 90°E from 11.5°S to 58.1°N in cases 1 and 4 are shown in Fig. 5d and b, respectively. In case 1, ridges of the waves appear over the deepest ripple with the amplitude decreasing with height. A local maximum of surface pressure appears at the deepest ripple. In case 4, this local maximum of surface pressure does not exist. An inter-comparison has proved that the deep ripples may cause a spurious short wave, especially in the surface pressure field.

The cross section of the meridional circulation in summer along 90°E from 11.5°S to 58.1°N in cases 1 and 4 are represented in Fig. 6a and b, respectively. By comparing Fig. 6a and b, subsidence appears over the deepest ripple in case 1 and strong upward motion over the same point exists in case 4. Obviously, the deep ripple produces downward motion and prevents upward motion, whereas strong upward motion instead of subsidence appears when the ripple is removed.

Precipitation in June—August in case 4 is shown in Fig. 7d. In this period, the precipitation difference between cases 1 and 4 is more apparent than in December—February. In case 4, an unrealistic splitting of monsoon precipitation existing in case 1 is prevented and the maximum center of precipitation is removed to Southeast Asia. The precipitation difference of monsoon between cases 1 and 4 appears because the deepest ripple produces subsidence which suppresses rainfall (see Fig. 6a, b). It clearly indicates that the disappearance of deep ripples due to smoothing allows for strong upward motion,

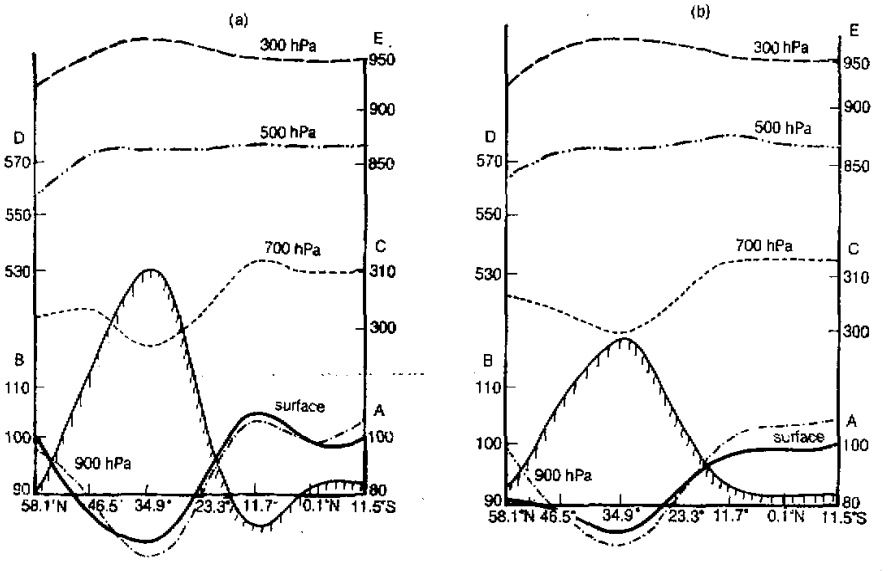

Fig. 5. Geopotential heights along 90°E from 11.5°S to 58.1°N. (a) case 1 for northern summer; and (b) case 4 for northern summer. A is the axis of the coordinate at surface (units: hPa); B, C, D and E are axes of coordinates at 900, 700, 500 and 300 hPa, respectively (units: 10 gpm).

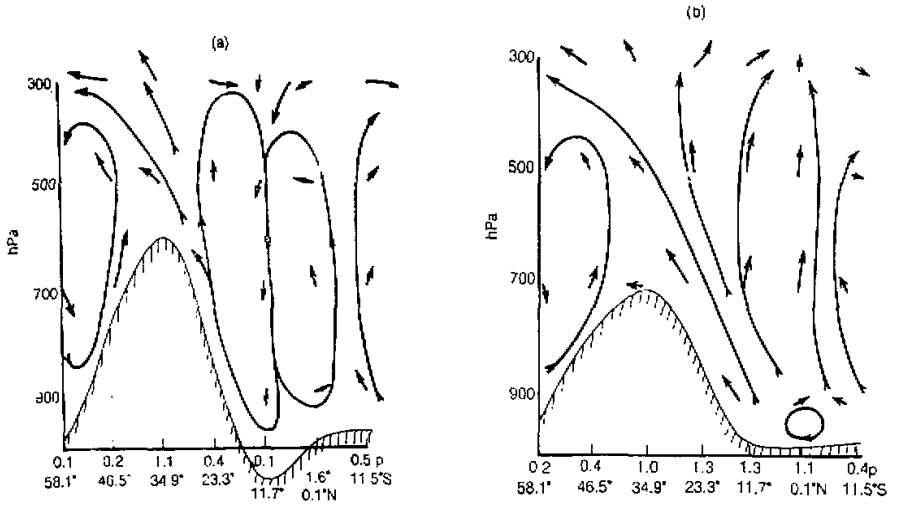

Fig. 6. Distribution of meridional circulation along 90°E from 11.5°S to 58.1°N. p, precipitation (cm/d). (a) case 1 for northern summer; and (b) case 4 for northern summer.

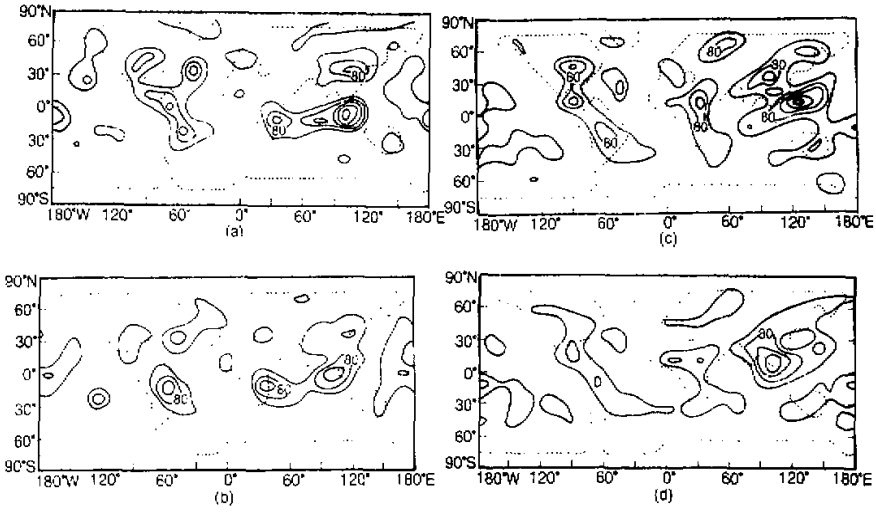

Fig. 7. Distribution of time-mean precipitation (10^{-1} mm/d). Contour intervals, 40×10^{-1} mm/d. (a) case 1 for northern winter; (b) case 4 for northern winter; (c) case 1 for northern summer; and (d) case 4 for northern summer.

causing rainfall, and avoids an unrealistic splitting of monsoonal precipitation (Fig. 7d).

The cross sections of the geopotential heights in winter along 90°E from 11.5°S to 58.1°N in cases 1 and 4 show that, as previous description in June—August, and apparent wave peak of surface pressure appears at the deepest ripple in case 1, whereas in case 4, the

wave peak disappears (figures omitted). The simulated geopotential height field in December—February also shows that there is a spurious high system over the deepest ripple area as that in June—August.

The cross sections of the meridional circulaton in winter along 90°E from 11.5°S to 58.1°N in cases 1 and 4 show that strong subsidence appears over the deepest ripple in case 1, and the downward motion over the same point is much weaker in case 4 than that in case 1 (figure omitted). These results confirm the conclusion described above.

Precipitation in cases 4 and 1 are shown in Fig. 7a and b, respectively. A great difference between cases 1 and 4 appears over the sub-continent of South Asia, that is, two main precipitation areas, which are respectively located over China and over the tropical Pacific Ocean, split over the sub-continent in case 1, but they are prevented from splitting in case 4. Clearly, the deepest ripple area over the South Asian, sub-continent the Arabian Sea and the Bay of Bengal causes strong subsidence, thus preventing the evident rainfall in the area. The distribution of meridional circulation along 90°E in cases 4 and 1 further indicates that the precipitation difference between cases 4 and 1 is caused by the deepest ripple area in case 1 and the raised orography due to smoothing in case 4.

V. SUMMARY AND CONCLUSIONS

In order to investigate the impact of smoothed orography and the spurious orographic ripples on simulations, numerical experiments with three different orography specifications are performed. The comparisons of the general circulation experiments in cases 3 and 4 with that in case 1 leads to the following conclusions:

(1) In winter, the spurious low over the Tibetan Plateau and the Siberian high in the lower troposphere are weakened in the model with smoothed orography, while the Siberian ridge is strengthened and the North American trough deepened at 300 hPa; in summer, geopotential heights at 900 hPa in the region of 45°N—60°N and 0°E—100°E, the South Polar area and the west coast of southern Africa are decreased by the smoothed orography, whose effect on geopotential heights is more pronounced in winter half-year than that in summer half-year.

(2) In winter, smoothed orography weakens the westerly jet in the upper troposphere in the Asian region along 30°N—50°N and the zonal wind in the lower troposphere north of 50°N, but stengthens the westerly jet in North America and zonal wind in the upper troposphere north of 50°N; in summer, smoothed orography has an influence on easterly in southern North America and northern Asia.

(3) There exist apparent regional characteristics of the effects of smoothed orography on meridional wind and vertical motion, and such effects are more pronounced in winter than in summer.

(4) Smoothed orography has a significant influence on temperature field throughout the troposphere in winter and summer, but it is more evident in the upper troposphere than in the lower one.

(5) In case 3, the unrealistic split of precipitation area in Asia, which appears in case 1, is improved.

On the whole, smoothing topography has important influences on the simulation in the low-resolution spectral model by decreasing the magnitude and extent of ripple points and reducing the heights of mountains. Consequently, some aspects of the simulation in the

smoothed mountain case are significantly improved, especially in northern winter.

(6) The deep ripples produce spurious a high pressure system on the surface, especially south of Tibet, and the associated subsidence suppresses rainfall and causes an unrealistic splitting of the precipitation area in northern winter and summer in Asia. The removal of the deep ripples by smoothing allows for strong upward motion to exist, eliminating the unrealistic splitting of precipitation area in Asia.

The authors wish to thank Dr. Akira Kasahara at NCAR for his review and constructive comments of this research and Dr. Robert Gallimore for his comments on the topography smoothing procedures. This research was sponsored by the Climate Dynamics Research Division, National Science Foundation through NSF Grant ATM 81-13464. Computing support by the National Center for Atmospheric Research is also gratefully acknowledged. NCAR is sponsored by the National Science Foundation.

REFERENCES

Arakawa, A., and Lamb, V.R. (1981), A potential enstrophy and energy conserving scheme for the shallow water equations, *Mon. Wea. Rev.*, **109**: 18–36.

Bourke, W. et al., (1977), Global modeling of atmospheric flow by spectral methods, *Methods in Computational Physics*, Vol. 17, *General Circulation Models of the Atmosphere, Academic Press*, New York, 267–323.

Chervin, R.M., and Schneider, S.H. (1976), On determining the statistical significance of climate experiments with general circulation models, *J. Atmos. Sci.*, **33**: 405–412.

Gates, W.L., (1984), The effects of large-scale mountains on the atmospheric general circulation and climate with special reference to eastern Asia, Report No. 50, Climatic Research Institute, Oregon State University, Corvallis, Oregon.

Jenne, R.L., (1975), Data sets for meteorological research, NCAR-TN/IA-111, Boulder, Co., 194pp.

McAvaney, B.J. et al. (1978), A global spectral model for simulation of the general circulation, *J. Atmos. Sci.*, **35**: 1557–1583.

Ni Yunqi (1986), Comparative study of computational stability between primitive equations in the p coordinate and the sigma coordinate (will be submitted).

Ni Yunqi, Otto-Bliesner, B.L. and Houghton, D.D. (1986), The sensitivity of numerical simulation to orography specification in the low resolution spectral model——Part I: The effects of orography on the general atmospheric circulation, *adv. Atmos. Sci.*, **4**: 1–14

Otto-Bliesner, B.L., Branstator, G.W. and Houghton, D.D. (1982), A global low-order spectral general circulation model, Part I: formulation and seasonal climatology, *J. Atmos. Sci.*, **39**: 929–948.